



Hydrodynamic planetary thermosphere model:

2. Coupling of an electron transport/energy deposition model

Feng Tian,¹ Stanley C. Solomon,¹ Liying Qian,¹ Jiuhou Lei,¹ and Raymond G. Roble¹

Received 15 November 2007; revised 14 March 2008; accepted 5 May 2008; published 15 July 2008.

[1] An electron transport/energy deposition model is expanded to include atomic nitrogen and is coupled with a 1-D hydrodynamic thermosphere model. The coupled model is used to investigate the response of the Earth's thermosphere under extreme solar EUV conditions and is compared with previous studies. It is found that (1) the parameterization of Swartz and Nisbet (1972) underestimates the ambient electron heating by photoelectrons significantly in the upper thermosphere of the Earth under conditions with greater than 3 times the present solar EUV irradiance; (2) the transition of the Earth's thermosphere from a hydrostatic equilibrium regime to a hydrodynamic regime occurs at a smaller solar EUV flux condition when enhanced, more realistic, and self-consistent, ambient electron heating by photoelectrons is accounted for; (3) atomic nitrogen becomes the dominant neutral species in the upper thermosphere (competing against atomic oxygen) under extreme solar EUV conditions, and the electron impact processes of atomic nitrogen are important for both the chemistry and energetics in the corresponding thermosphere/ionosphere; (4) N^+ remains a minor ion compared to O^+ , even when atomic nitrogen dominates the exobase; and (5) adiabatic cooling does not play an important role in electron gas energy budget. These findings highlight the importance of an electron transport/energy deposition model when investigating the thermosphere and ionosphere of terrestrial planets in their early evolutionary stages.

Citation: Tian, F., S. C. Solomon, L. Qian, J. Lei, and R. G. Roble (2008), Hydrodynamic planetary thermosphere model: 2. Coupling of an electron transport/energy deposition model, *J. Geophys. Res.*, 113, E07005, doi:10.1029/2007JE003043.

1. Introduction

[2] Geological evidences show that the atmospheric composition of early Earth was different from that of today. The present atmospheres of terrestrial planets in our solar system are different from each other. These spatial and temporal variabilities require a generalized planetary atmosphere model, which does not rely on any specific parameterization methods developed for any particular planetary atmospheres, in order to understand the long-term evolution of planetary atmospheres. To reach such an ideal goal, certainly, is difficult and cannot be accomplished all at once.

[3] Tian *et al.* [2008] (hereinafter referred to as paper 1) developed the first 1-D, multicomponent, hydrodynamic model (hereinafter referred to as model 1) to investigate the response of the thermosphere/ionosphere of a hypothetical Earth-like planet to extreme solar EUV inputs. It is found that the Earth's thermosphere would have experienced a transition from hydrostatic equilibrium regime to hydrodynamic flow regime when exposed to extreme solar EUV conditions [Tian *et al.*, 2008]. The chemical scheme in model 1 include chemical reactions found in a wide range of planetary atmospheres (Earth, Venus, Mars, and giant plan-

ets) and the hydrostatic equilibrium assumption has been abandoned in model 1 in order to correctly characterize the hydrodynamic nature of planetary thermospheres under extremely strong solar EUV conditions. These features make model 1 more suitable than other existing models, which contains specific chemical schemes designed for particular planetary atmospheres and often use hydrostatic equilibrium as an underlying assumption, to investigate the long-term evolution of a broad range of planetary atmospheres. Despite these advances, model 1 still relies on parameterizations developed in present Earth's thermosphere in the following aspects: (1) ionizations, excitations, and dissociations by electron impact processes and (2) heating of ambient electrons by photoelectrons and secondary electrons. It is unclear whether or not these parameterizations are applicable to planetary atmospheres with different composition patterns and/or planetary atmospheres under the influence of different external environments (such as different solar EUV levels, different energetic particle injection fluxes). In order to treat both aspects self-consistently, an energetic electron production/transport model is needed. In this paper we expand an existing energetic electron transport/energy deposition model (the GLOW model [Solomon *et al.*, 1988; Bailey *et al.*, 2002]) and couple it with model 1. The coupled model is used to investigate the behavior of the Earth's thermosphere as well as various photon and electron impact processes in the thermosphere under extreme EUV conditions.

¹High Altitude Observatory, National Center for Atmospheric Research, Boulder, Colorado, USA.

Table 1. Fitting Parameters for the Electron Impact Ionization Cross Sections of Atomic Nitrogen in Equations (1)–(6)

I	K	J	T_s	T_a	T_b	Γ_s	Γ_b
14.55	2.49	3.62	7.05	3450	178	19.5	-0.815

[4] In paper 1, we discussed the importance of adiabatic cooling, associated with the hydrodynamic flow of one single background fluid including both neutral and ion species, to the neutral gas energy budget. Since quasi-neutrality is assumed in model 1, electrons should be moving together with ions at the same velocity, if not greater. However, the adiabatic cooling associated with the bulk motion of electrons is ignored in the electron gas energy equation, which induces significant uncertainties. In this paper we solve the complete electron energy equation to address this issue.

2. Model Descriptions

[5] The GLOW model is an energetic electron transport and energy deposition model developed for the Earth's thermosphere [Solomon *et al.*, 1988; Bailey *et al.*, 2002]. A version of it has been applied to Venus [Alexander *et al.*, 1993]. We use the Earth version (containing three major species O, O₂, and N₂) as the base for the expansion. For details of the GLOW model, readers are referred to Solomon *et al.* [1988] and Bailey *et al.* [2002]. The following is a brief description.

[6] The GLOW model treats the transport of energetic electrons (photoelectrons, secondary electrons, and precipitated electrons) using a two-stream approach following Nagy and Banks [1970]. Comparison of the two-stream method to comprehensive Monte Carlo, hybrid, and multi-stream calculations for auroral fluxes is shown by Solomon [1993, 2001]. The two-stream method was found to be an adequate approximation unless pitch angle distributions were highly anisotropic. Although we are not aware of similar model comparisons for the photoelectron case, since the source function for photoelectrons is nearly isotropic, it is expected that the two-stream method is an even better approximation. Comparisons between photoelectron flux measurements and models [e.g., Solomon *et al.*, 2001] have also established the validity of this approach. Collisions between energetic electrons with ambient electrons and three major neutral gases (O, O₂, and N₂) are included. Elastic collisions influence the energetic electron fluxes (both upward and downward) directly while inelastic collisions (ionization, excitation, and dissociation) lead to the cascade of energetic electrons to less energetic electrons. Energetic electrons are divided into energy bins and the transport equation is solved for the highest energy bin first and the lowest energy bin last to fully account for the cascade processes. The GLOW model has been used to analyze and explain the observed O¹D airglow emissions in the Earth's thermosphere [Solomon and Abreu, 1989]. Parameterization methods (for the contributions to ionization, excitation, and dissociation by electron impact processes) developed on the basis of the GLOW model have been employed by general circulation models such as the

Thermosphere Ionosphere Electrodynamics General Circulation model (TIE-GCM) [Solomon and Qian, 2005].

[7] In model 1, it is found that atomic N becomes the dominant species near the exobase under extreme solar EUV conditions, which makes the ionization and excitation of N important in the aspects of both chemistry and energetics. In this work, the electron impact ionization and excitation of N atoms are added in the GLOW model so that the model can be applied to extreme solar EUV conditions. Photoionization and absorption cross sections of N are from Fennelly and Torr [1992]. The energy of photoelectrons is calculated by subtracting the ionization threshold energy from that of the photon. Secondary electrons are important for further ionization, excitation, and dissociations. In order to calculate the transport and production of secondary electrons accurately, it is important to obtain their distributions at sources. To accomplish this, the practical approach employed by the GLOW model is to fit the electron impact ionization cross section data with one analytical expression and then apply the fitting parameters to another analytical expression to obtain the distribution of the secondary electrons. For the electron impact ionization processes, the following analytical expressions are used [Green and Sawada, 1972; Sawada *et al.*, 1972; Jackman *et al.*, 1977]:

$$\begin{aligned}\sigma_i(E) &= \int_0^{T_m} S_i(E, T) dT \\ &= A(E)\Gamma(E) \left[\tan^{-1} \left(\frac{T_m - T_0}{\Gamma} \right) + \tan^{-1} \left(\frac{T_0}{\Gamma} \right) \right],\end{aligned}\quad (1)$$

$$S_i(E, T) = \frac{A(E)\Gamma^2(E)}{[T - T_0(E)]^2 + \Gamma^2(E)},\quad (2)$$

with

$$A(E) = \sigma_0 \frac{K}{E} \log \left(\frac{E}{J} \right),\quad (3)$$

$$\Gamma(E) = \Gamma_s E / (E + \Gamma_b),\quad (4)$$

$$T_0(E) = T_s - \frac{T_a}{E + T_b},\quad (5)$$

and

$$T_m = (E - I)/2.\quad (6)$$

In equations (1)–(6), $\sigma_0 = 10^{-16}$ cm², E is the energy of the primary electrons, T is the energy of secondary electrons, I is the ionization threshold of the gas, $\sigma_i(E)$ is the ionization cross section and $S_i(E, T)$ is the differential ionization cross section. All other undefined variables in these equations are adjustable fitting parameters. The electron impact ionization cross sections of atomic nitrogen by Avakyan *et al.* [1998] are fitted using equation (1) and the fitting parameters are included in Table 1.

Table 2. Fitting Parameters for the Electron Impact Excitation Cross Sections of Atomic Nitrogen in Equation (7)

Excited States	W	A	Ω	γ	ν
2^1D^0	2.386	0.0540	1.35	1.00	1.60
2^1P^0	3.576	0.0325	1.48	0.60	1.04
$3s^4P$	10.330	0.4124	0.69	1.02	2.00
$3s^2P$	10.687	0.1654	1.90	1.01	1.08
$2p^4\ ^4P$	10.924	0.1470	0.70	4.19	5.57

[8] For electron impact excitation processes, the analytical expression of *Green and Stolarski* [1972] is used:

$$\sigma(E) = \frac{q_0 A}{W^2} \varepsilon^{-\Omega} \Phi(\varepsilon), \quad (7)$$

with $\Phi = (1 - \varepsilon^{-\gamma})^\nu$ and $\varepsilon = E/W$. Here $q_0 = 6.514 \times 10^{-14}$ eV² cm², and E is the energy of the incident electron. All other undefined variables are fitting parameters and are included in Table 2.

[9] For electron impact excitation, we include the following excited states into consideration: $N(2^1D^0)$, $N(2^1P^0)$, $N(3s^4P)$, $N(2p^4\ ^4P)$, and $N(3s^2P)$. The cross sections of the first 4 excited states are taken from *Tayal and Zatsarinny* [2005]. For the cross sections of $N(4^1S^0) \rightarrow N(3s^2P)$, we use

the cross sections of *Stone and Zipf* [1973], which are from emission measurements. Because the Lyman alpha calibration standard changed after the measurements were taken, the electron impact excitation cross sections of O atoms from the same authors need to be adjusted downward by as much as a factor of 2.8 [*Zipf and Erdman*, 1985]. Similar adjustments have not been reported for N atoms. The calculated peak cross sections of *Tayal and Zatsarinny* [2005] for $N(4^1S^0) \rightarrow N(3s^4P)$ and $N(4^1S^0) \rightarrow N(2p^4\ ^4P)$ are smaller than those reported in the work by *Stone and Zipf* [1973] by about factors of 4.5 and 5.2. Because the emission measurements include the contribution of cascade from other excited states, we take the freedom to adjust the cross section of *Stone and Zipf* [1973] downward by a factor of 2.8. Sensitivity tests in extreme solar EUV cases show that the simulation results are not sensitive to this adjustment. Because the cross sections of *Stone and Zipf* [1973] is for the emission line of 1744 Å, they need to be multiplied by 2.79 to obtain the electron impact cross sections of $N(4^1S^0) \rightarrow N(3s^2P)$ [*Meier*, 1991].

[10] Through experiments, we obtained the fitting parameters for electron impact ionization and excitation of N summarized in Tables 1 and 2. The cross section data and the analytical expressions with the fitting parameters are shown in Figure 1. Note that these fitting parameters may

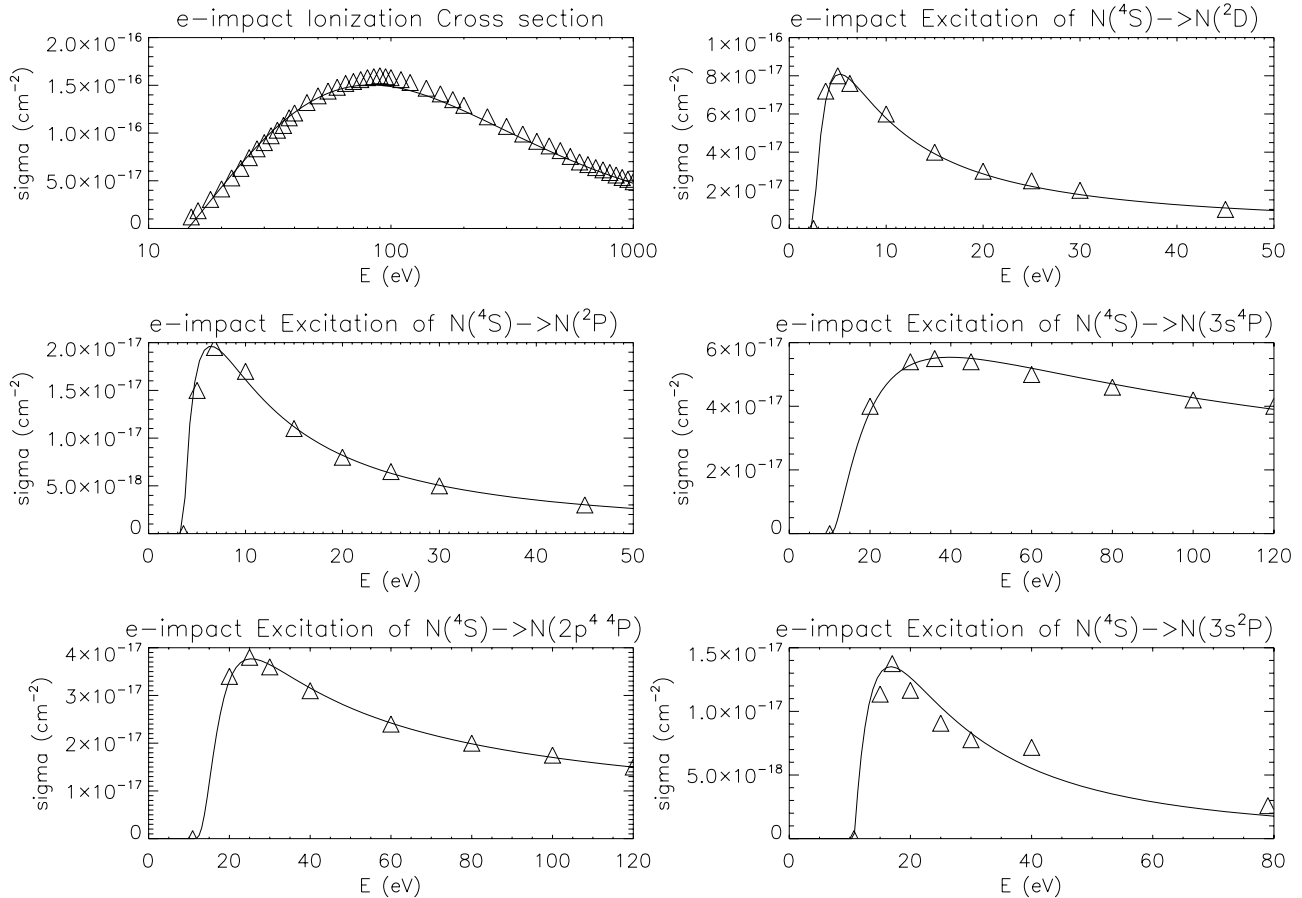


Figure 1. The ionization and excitation cross sections of atomic nitrogen. The triangles are the data collected from the references cited in the main text. The curves are obtained by applying equations (1)–(7) with the fitting parameters in Table 1 and 2.

have errors because (1) the fittings are not perfect and (2) electron impact excitation cross sections are read from figures in the corresponding references. A better approach would be to use cross section tables instead of fitting parameters to analytical expressions, which will be useful future work. Elastic collisional cross sections and backscattering probabilities (both elastic and inelastic) of N are assumed to be the same as those of O. Auger ionization effect is ignored for N.

[11] The expanded GLOW model is called by model 1 every 10 time steps in order to save computation time. Sensitivity tests show that the simulation results do not change when increasing the calling frequency of GLOW. Each time GLOW is called, it takes the density profiles of major species (O, O₂, N, and N₂) and the electron temperature profile from model 1 as input. Then the ionization, excitation, and dissociation rates of the major species in both electron impact processes and photon processes are computed and fed back to model 1. The electron gas heating rate due to the collisions between photoelectrons and ambient electrons is also computed in GLOW and fed to model 1. The coupled model evolves in time until a steady state solution is found.

[12] For electron gas energy equation, we start from that given by *Schunk and Nagy* [2000]:

$$\begin{aligned} \frac{3}{2}n_e k \frac{\partial T_e}{\partial t} = & -n_e k T_e \nabla \cdot \vec{u}_e - \frac{3}{2}n_e k \vec{u}_e \cdot \nabla T_e - \nabla \cdot \vec{q}_e \\ & + \sum Q_e - \sum L_e - \sum_i \frac{\rho_e \nu_{ei}}{m_i} 3k(T_e - T_i) \\ & - \sum_n \frac{\rho_e \nu_{en}}{m_n} 3k(T_e - T_n). \end{aligned} \quad (8)$$

Here k is the Boltzmann constant, n_e is the electron density, T_e is the electron temperature, u_e is the bulk motion velocity of the electron gas, q_e is the heat flux, $\sum Q_e$ is the sum of the external heating rates, and $\sum L_e$ is the sum of the inelastic cooling rates. The last two terms on the right-hand side of equation (8) are the elastic collisional cooling of electron gas by ions and neutrals.

[13] Because of the possible strong expansion of the planetary thermosphere, distance from the planet center r instead of altitude z is normally used. In the 1-D spherical isotropic case, equation (8) can be simplified to the following format:

$$\begin{aligned} \frac{3}{2}n_e k \frac{\partial T_e}{\partial t} = & -n_e k T_e \frac{\partial(u_e r^2)}{r^2 \partial r} - \frac{3}{2}n_e k u_e \frac{\partial T_e}{\partial r} + \frac{\partial}{\partial r} \left(\lambda_e r^2 \frac{\partial T_e}{\partial r} \right) \\ & + \sum Q_e - \sum L_e - \sum_i \frac{\rho_e \nu_{ei}}{m_i} 3k(T_e - T_i) \\ & - \sum_n \frac{\rho_e \nu_{en}}{m_n} 3k(T_e - T_n). \end{aligned} \quad (9)$$

Here r is the distance from the center of the planet, $\lambda_e = 7.7 \times 10^5 T_e^{5/2} \text{ eV cm}^{-1} \text{ s}^{-1} \text{ K}^{-1}$ is the thermal conductivity [*Schunk and Nagy*, 2000]. Note that this thermal conductivity expression is for fully ionized plasma (Spitzer conductivity), which does not apply to the lower thermosphere. However, in the lower thermosphere the electron temperature profile is tied by neutral temperature profiles due to frequent collision. Thus the error introduced by using

the Spitzer conductivity is negligible. On the other hand, when exposing the thermosphere to extreme EUV conditions, the thermosphere/ionosphere should become more ionized, which approves the usage of the Spitzer conductivity. We neglected the effect of dip angle (the angle between the magnetic field lines and the horizontal direction) on thermal conductivity in equation (9). We note that this is a justifiable assumption at the polar and high-latitude region only. In middle latitude and equatorial region, the effect of ignoring the dip angle is to overestimate the thermal conduction term (the third term on the right hand side) in equation (9) in the vertical direction. In the Earth's lower thermosphere, thermal conduction is not important due to efficient collisions between neutrals, ions, and electrons. Therefore neglecting the dip angle in equation (9) should not affect the electron temperature in the lower thermosphere significantly. In the upper thermosphere, all other terms in equation (9) become negligible and the electron energy balance is controlled by the thermal conduction term, $(\partial/\partial r)[\lambda_e r^2 (\partial T_e/\partial r)] \cong 0$, neglecting the dip angle should not affect the electron temperature significantly either. Thus the errors introduced by neglecting the dip angle should be important only in middle altitudes. We note that the horizontal conductivity, which becomes important near the equatorial region, cannot be accounted for due to the 1-D global-average nature of the model.

[14] The first two terms on the right-hand side of equation (2) are the adiabatic expansion and the advection cooling terms. In this paper we refer to the sum of the two terms as adiabatic cooling. The adiabatic cooling terms are normally negligible in the terrestrial ionosphere [*Schunk and Nagy*, 2000] and are ignored in paper 1. However, because paper 1 showed that the adiabatic cooling associated with the hydrodynamic flow can become the dominant neutral gas cooling mechanism under extreme solar EUV conditions, the significance of adiabatic cooling to the electron gas in similar situations needs to be investigated. Most work in this paper is done by assuming that the bulk motion velocity of electrons is the same as that of neutral and ion gases. The motion of electrons should be constrained by the magnetic field. As a result, the bulk motion velocity of the electron gas should be smaller than those of neutral gases in the middle-low-latitude regions, and the adiabatic cooling effect on the electron gas should be more limited than what is assumed here. In section 4 the results of sensitivity tests in an extreme case in which the electrons are assumed to be static are discussed.

[15] To validate that the GLOW model has been properly coupled with the hydrodynamic thermosphere model, we compare the profiles of neutral temperature, electron temperature, and electron density calculated in the present work (solid curves) under solar minimum and solar maximum conditions with their counter parts (dashed curves) in paper 1 (Figure 2). The dotted curves are the temperature profiles from the Naval Research Laboratory mass spectrometer incoherent scatter radar extended model [*Hedin*, 1991]. For simplicity, the atmospheric temperature and composition at the lower boundary (~ 97 km) is assumed to be the same as that of present Earth. Both the neutral and the electron temperature in the present work are similar to, but somewhat higher than, the results in paper 1. The electron densities in the upper thermosphere decreases slightly in the

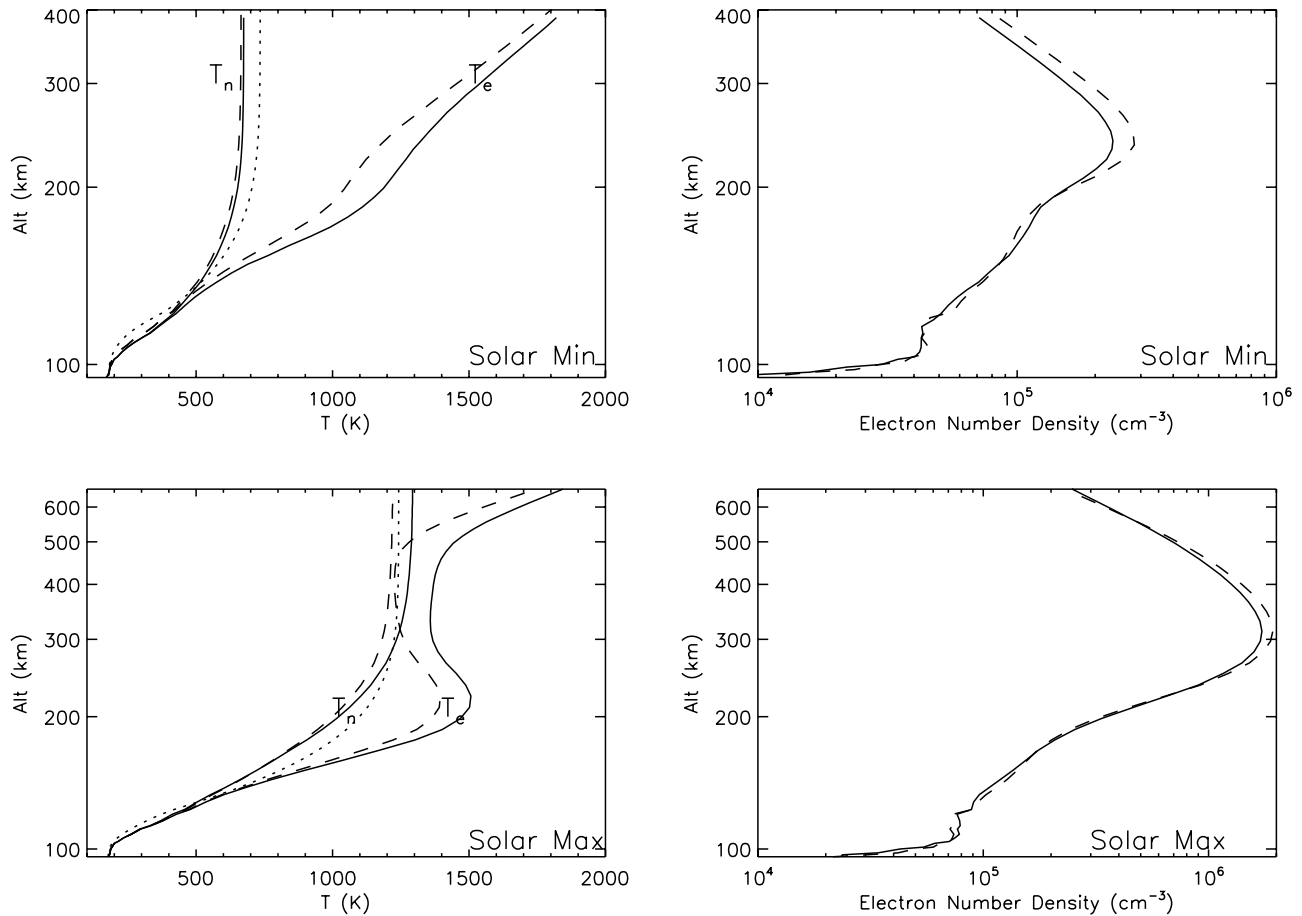


Figure 2. Comparisons between the temperature and density profiles in the present work with those in paper 1 under solar maximum and minimum conditions. Dashed curves are from paper 1. Solid curves are from the present work. The dotted curves in Figures 2 (top left) and 2 (bottom left) are from the MSIS-00 model [Hedin, 1991].

present work than in paper 1, which can be related to increased recombination reaction rates due to the increase of electron temperature. The increase of neutral and electron temperature in the present work can be explained by stronger neutral and electron heating functions provided by the GLOW model than those provided by the parameterization methods used in model 1, although both the present work and the previous work can be seen as in good agreement with the measurements considering the global mean nature of the models. In the next section, it is shown that the present model produces results significantly different from those of model 1 under extreme solar EUV conditions and the significance of coupling the GLOW model with the hydrodynamic thermosphere model becomes apparent. The profiles of mass density and the number densities of various species (both ion and neutral) of the Earth's thermosphere under solar maximum and minimum conditions in the present work are similar to those in paper 1.

[16] Figure 3 shows the profiles of photoionization, photodissociation, electron impact dissociation, and photoelectron enhancement factors (the ratio between electron impact ionization rates and photoionization rates) calculated in the present model under solar minimum condition ($F_{107} = 70$).

The solar zenith angle is 60° , and the dip angle used in the GLOW calculations is 22.7° . Sensitivity tests show that our simulation results are not sensitive to the specific choice of the dip angle in the GLOW calculations. The photoionization and photodissociation rates in Figure 3 have intermediate values between their counterparts from Solomon and Qian [2005], which are obtained by applying the GLOW model for either overhead Sun or high solar zenith angle (85°) condition. For example, the peak photoionization rate of N_2 is $\sim 2000 \text{ cm}^{-3} \text{ s}^{-1}$ and $100 \text{ cm}^{-3} \text{ s}^{-1}$ for the overhead Sun and the high solar zenith angle (85°) condition, respectively, while the peak photoionization rate of N_2 in Figure 3 is $\sim 500 \text{ cm}^{-3} \text{ s}^{-1}$. Another example, the peak photodissociation rates of O_2 by solar EUV flux is $\sim 6000 \text{ cm}^{-3} \text{ s}^{-1}$ and $\sim 400 \text{ cm}^{-3} \text{ s}^{-1}$ by Solomon and Qian [2005], while it is $\sim 1000 \text{ cm}^{-3} \text{ s}^{-1}$ in the present work. Both indicate that the GLOW model has been properly coupled with the thermosphere model. It is interesting to note that although the electron impact dissociation of N_2 (peak rate $\sim 1200 \text{ cm}^{-3} \text{ s}^{-1}$) is much stronger than the photodissociation of N_2 (peak rate $< 400 \text{ cm}^{-3} \text{ s}^{-1}$), its contribution to the O_2 dissociation (peak rate $\sim 1000 \text{ cm}^{-3} \text{ s}^{-1}$) is negligible because of the efficient dissociation of O_2 by

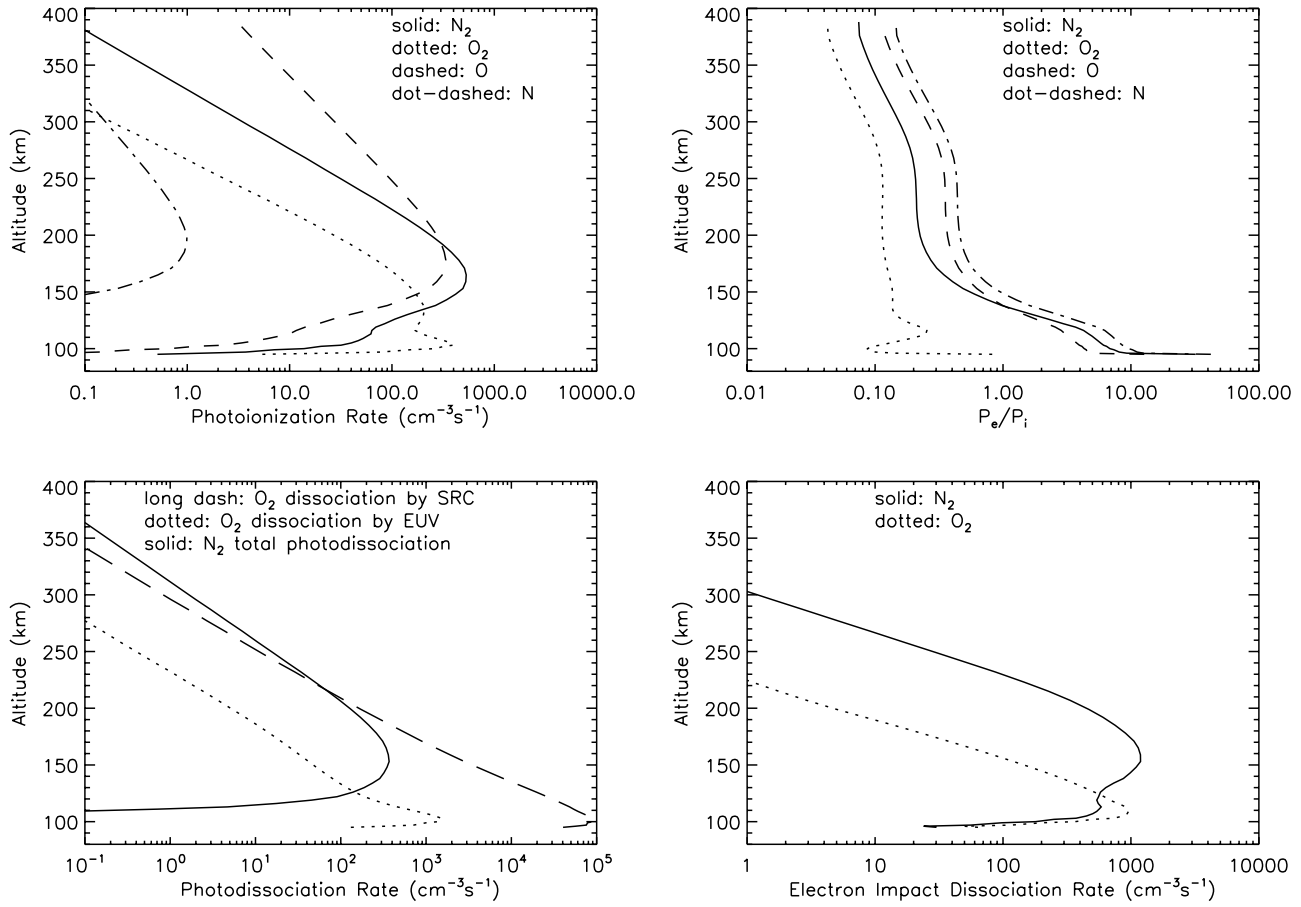


Figure 3. The profiles of photoionization, photodissociation, electron impact dissociation, and photoelectron enhancement factors calculated in the coupled model under solar minimum condition. The solar zenith angle is 60° and the dip angle is 22.7° . The long-dashed curve in Figure 3 (bottom left) represents the photodissociation of O_2 by the Schumann-Runge continuum. The dotted curve is the O_2 photodissociation by EUV photons. The solid curve is the total N_2 photodissociation rates by photons with wavelength $<1750 \text{ \AA}$.

the Schumann-Runge Continuum (with a peak rate of $10^5 \text{ cm}^{-3} \text{ s}^{-1}$), which dominates the dissociation of O_2 .

3. Thermosphere and Ionosphere Under Extreme Solar EUV Conditions

[17] Figure 4 shows the temperature profiles of the Earth's thermosphere under different solar EUV conditions in both the present work (red curves) and in paper 1 (blue curves). Paper 1 showed that the Earth's thermosphere experienced a transition from a hydrostatic equilibrium regime into a hydrodynamic regime, in which the adiabatic cooling associated with the hydrodynamic flow becomes the dominant cooling mechanism of the neutral gases in the upper thermosphere. A similar transition is found in this work and the shapes of the temperature profiles appear to be similar to those in paper 1. However, the thermospheres in this work are notably warmer than their counterparts in paper 1. In the $3.3\times$ present EUV case, the exobase temperature (T_{exo}) in this work is greater than 3000 K while in paper 1 it is slightly greater than 2000 K. T_{exo} in the $4.6\times$ present EUV case is $\sim 8000 \text{ K}$ in this work and is $\sim 3500 \text{ K}$ in paper 1. In fact, the temperature in the $4.6\times$ present EUV

case starts to drop slightly with altitude in the upper thermosphere, indicating that an increasingly important role of the hydrodynamic flow in the thermosphere and its associated adiabatic cooling effect. In paper 1 the same effect remains insignificant until the solar EUV flux reaches $\sim 5.3\times$ present EUV level. Thus it appears that the GLOW model is more efficient in heating the neutral gases than the parameterization methods used in paper 1. The thermosphere in the present work becomes transonic when exposed to solar EUV flux greater than $\sim 10\times$ present EUV and the numerical method employed here is not applicable in transonic hydrodynamic flow. Future work should be done to understand the response of the thermosphere to more extreme solar EUV conditions.

[18] Figure 5 shows the neutral gas heating rate and the contributions of different channels in both the solar maximum and the $4.6\times$ present EUV case. The profiles in the latter case can be seen as typical profiles for all extreme solar EUV condition cases. The neutral heating profiles in the solar maximum case are similar to those in previous works [Roble *et al.*, 1987; Roble, 1995]: heating from elastic collisional between electrons, ions, and neutrals (q_{en}) dominates the upper thermosphere and heating from

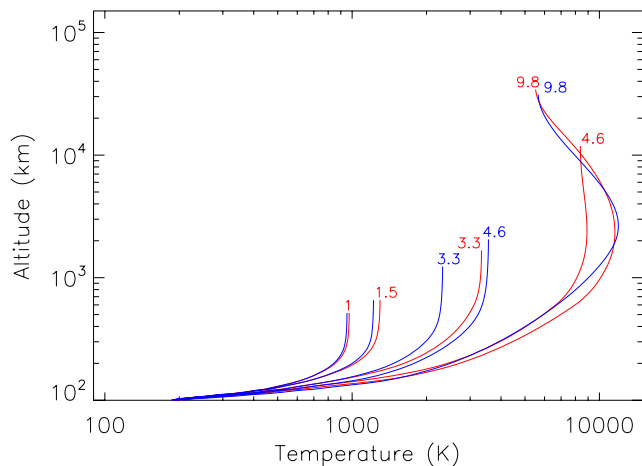


Figure 4. The temperature profiles of the Earth's thermosphere under different solar EUV conditions. The numbers (1, 1.5, 3.3, 4.6, and 9.8) represent the ratios between solar EUV fluxes and the present solar mean flux. The blue curves are from paper 1, and the red curves are from the present work.

exothermic chemical reactions (q_{chem}) dominates the lower thermosphere, with UV heating (q_{uv} , including SRC, SRB, Lyman alpha, and various bands of O_2 and O_3) as a complimentary heating source. Despite the fact that the

thermosphere in the high solar EUV case expands to 10,000 km altitude and the different net heating rates, the dominant neutral heating mechanisms at various parts of the thermosphere remain similar.

[19] Figure 5 shows that Joule heating is unimportant in all altitudes. Joule heating is included in the model by specifying an externally applied electric field (assumed constant with height) and calculating the Pedersen conductivity, similar to the treatment in the global mean model [Roble *et al.*, 1987; Roble, 1995]. Because the Pedersen conductivity increases and the atmosphere expand with increasing solar EUV energy input, the Joule heating contribution increases in magnitude. Whether or not this parameterization can be applicable to the much more expanded thermosphere/ionosphere of the Earth under extreme solar EUV conditions needs future investigations. To check the sensitivity of our model results against this uncertainty, the Joule heating is set to zero in a series of solar EUV cases and the results are plotted in Figure 10 as triangles. Comparing with the results with Joule heating, the exobase temperatures change by $\sim 5\%$.

[20] Figure 6 shows the density profiles of O and N under different solar EUV conditions. With increasing solar EUV fluxes, the number densities of both atomic oxygen and atomic nitrogen in the upper thermosphere increase dramatically. At 500 km altitude, the O and N densities are in the range of 10^7 and 10^5 cm^{-3} , respectively, under solar mean conditions. At the same altitude, the O densities are in the

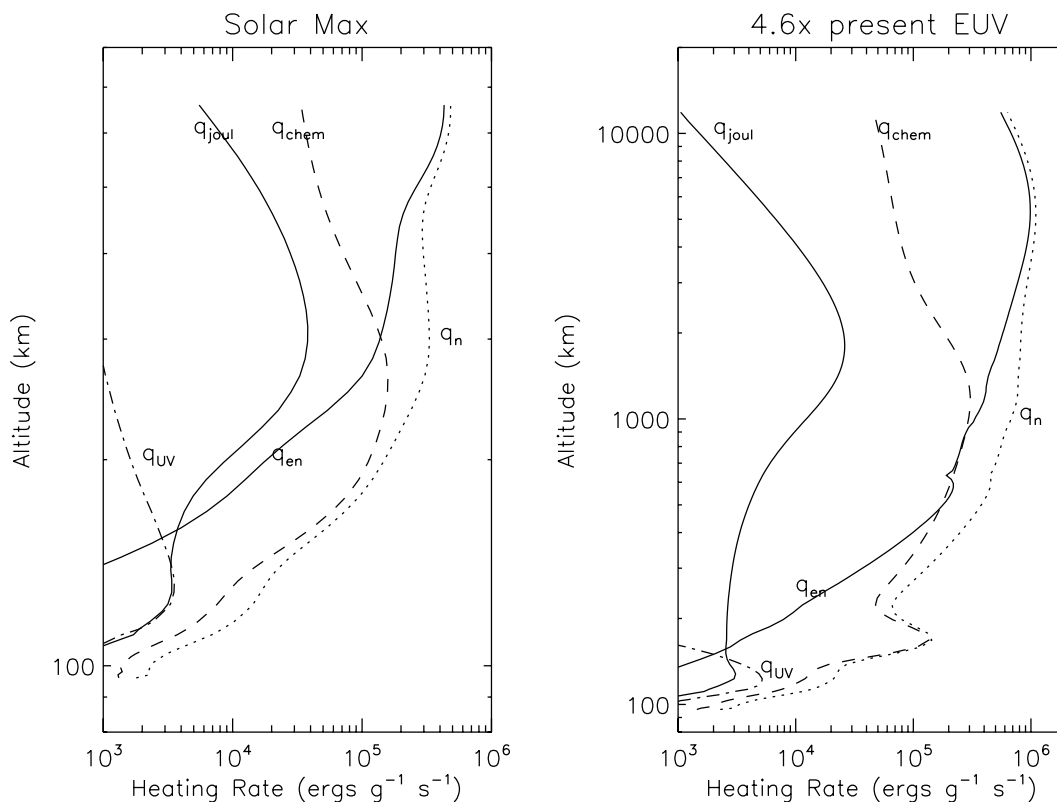


Figure 5. The contributions of different channels to the total neutral gas heating rate (q_n) in the solar maximum and the $4.6\times$ present EUV cases. Here q_{en} is the elastic collisions between electrons, ions, and neutrals, q_{chem} is the heating from exothermic chemical reactions, q_{uv} is the UV heating (including SRC, SRB, Lyman alpha, and various bands of O_2 and O_3), and q_{joul} is the Joule heating.

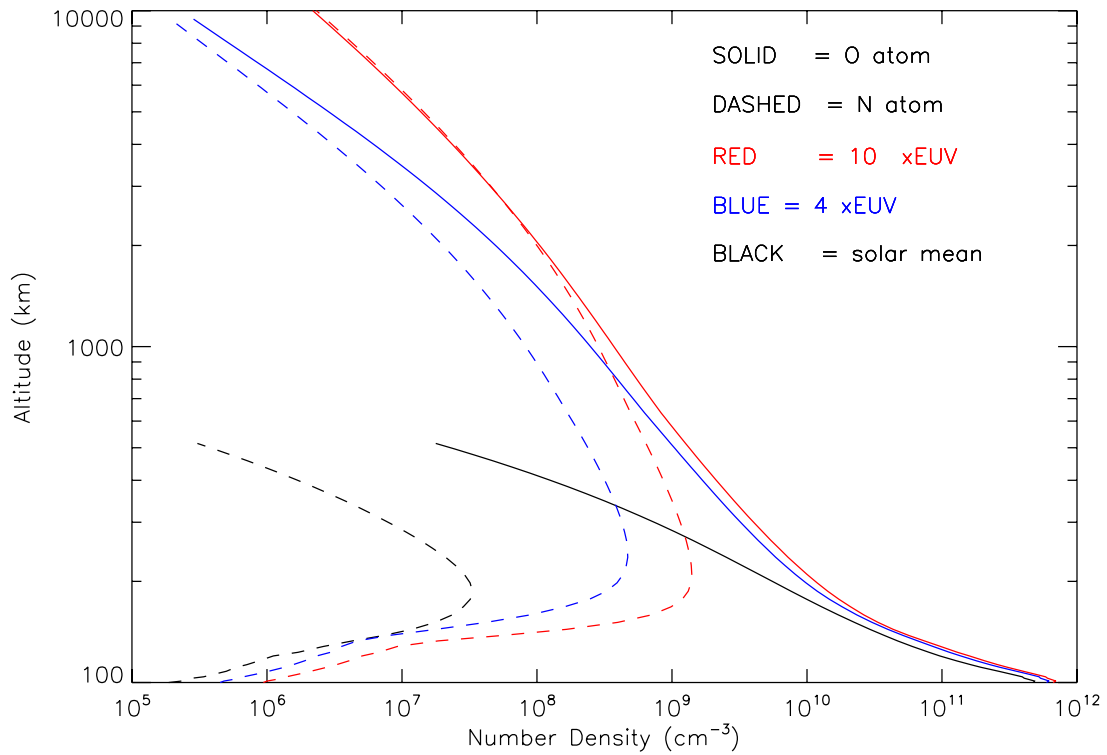


Figure 6. The density profiles of atomic oxygen (solid curves) and atomic nitrogen (dashed curves) under different solar EUV conditions.

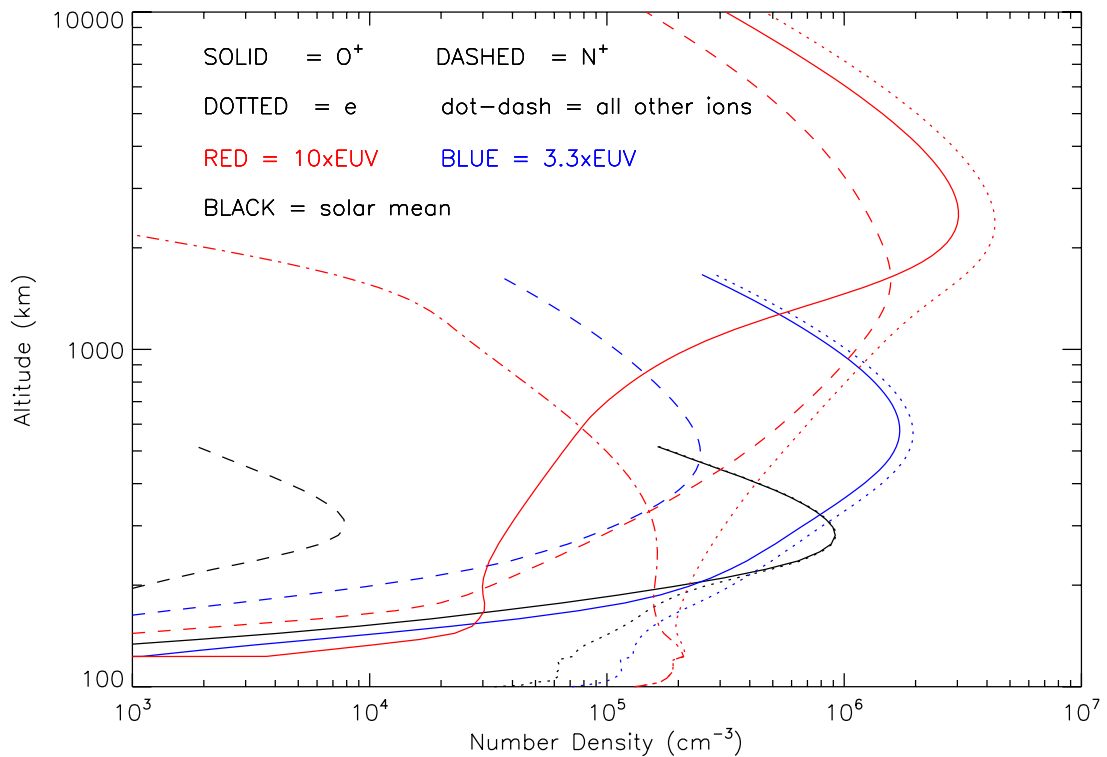


Figure 7. The density profiles of O⁺ (solid curves), N⁺ (dashed curves), and electrons (dotted curves) under different solar EUV conditions. The total density curves of all ions other than O⁺ and N⁺ in the 10× present EUV case is presented with the dot-dashed curve.

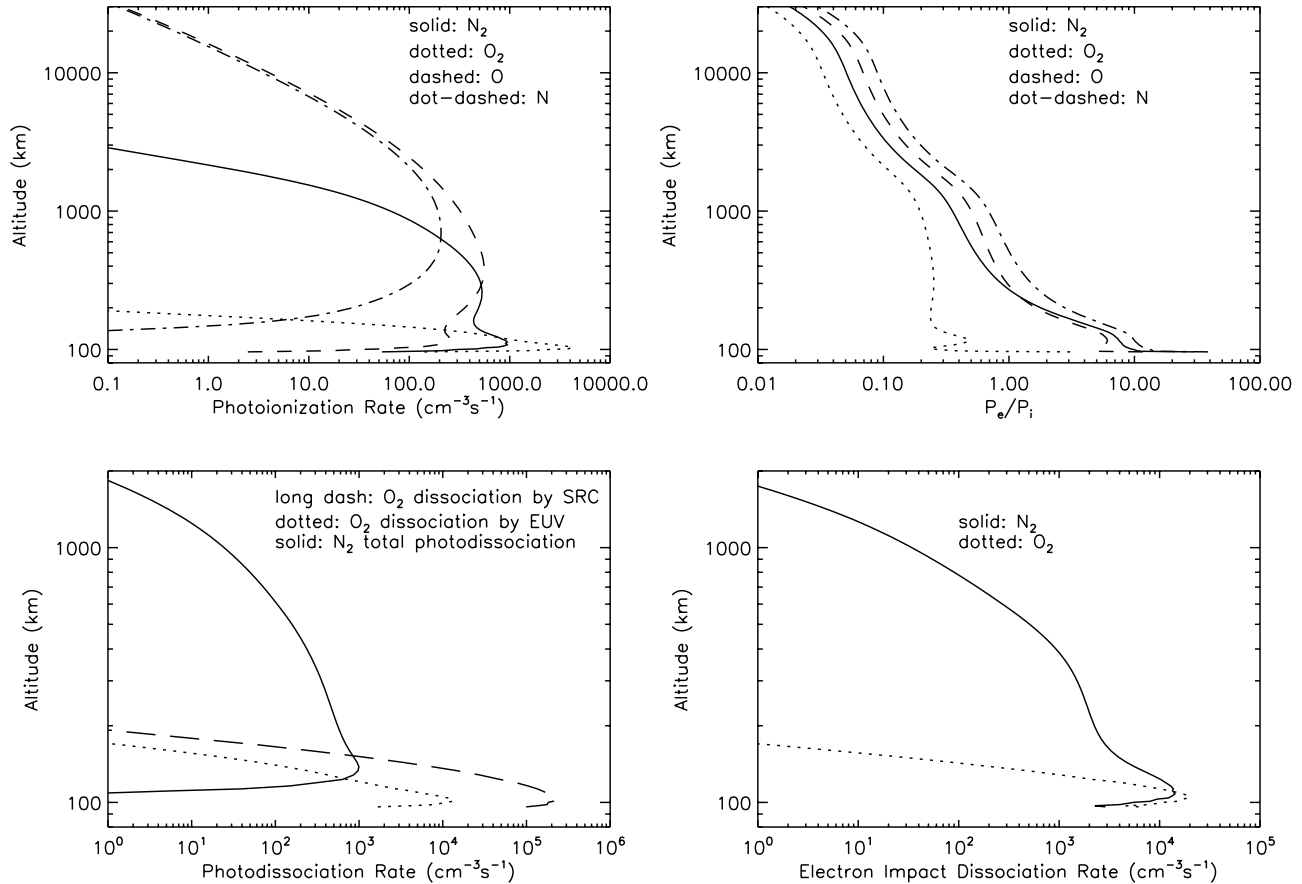


Figure 8. Profiles of photoionization, photodissociation, electron impact dissociation, and photoelectron enhancement factors calculated in the present work in the $10\times$ present EUV case. The solar zenith angle is 60° and the dip angle is 22.7° . The long-dashed curve in Figure 8 (bottom left) represents the photodissociation of O_2 by the Schumann-Runge continuum. The dotted curve is the O_2 photodissociation by EUV photons. The solid curve is the total N_2 photodissociation rate by photons with wavelength $<1750 \text{ \AA}$.

range of 10^9 cm^{-3} in the $4\times$ and $10\times$ present EUV cases. N density at 500 km altitude increases from $\sim 10^8 \text{ cm}^{-3}$ in the $4\times$ present EUV case to 10^9 cm^{-3} in the $10\times$ present EUV case. Because of more efficient dissociation of N_2 under $10\times$ present solar EUV condition, N density can become comparable to that of O in the upper thermosphere, both reaching $\sim 10^8 \text{ cm}^{-3}$ at $\sim 2000 \text{ km}$ altitude.

[21] Figure 7 shows the density profiles of O^+ , N^+ , and electrons under different solar EUV conditions. In solar mean condition, the N^+ density is about 2 orders of magnitude smaller than the O^+ density all through the thermosphere. In $3.3\times$ present EUV case, the difference between the two ion species has reduced to 1 order of magnitude. In the $10\times$ present EUV case, N^+ becomes the dominant ion species in the middle thermosphere (300 \sim 1000 km). The total density of all ions other than O^+ and N^+ is plotted for the $10\times$ present EUV case to demonstrate the region where N^+ dominates the ion population. Interestingly, N^+ density in the upper thermosphere ($>2000 \text{ km}$) is always smaller than that of O^+ by a factor of 2–3.

[22] Figure 8 shows the same contents with similar parameters as those in Figure 3 but is for the $10\times$ present EUV condition. The photoionization of N is similar to that

of O in the upper thermosphere because of the similar density of the corresponding atoms at high altitudes. Also in the upper thermosphere, the electron impact enhancement factor p_e/p_i reaches lower values (0.01 \sim 0.03) than that in solar minimum condition (0.04 \sim 0.2 as shown in Figure 3). This may be due to the high ratios between electron density (shown in Figure 7) and neutral density (shown in Figure 3) in the upper thermosphere in the $10\times$ present EUV case, which makes the interactions between photoelectrons and neutral species less efficient. The photodissociation and electron impact dissociation of O_2 are limited to the lower thermosphere ($<200 \text{ km}$), similar to the situation in present Earth's thermosphere. The dissociation of N_2 occurs in a much broader altitude range ($<1000 \text{ km}$).

4. Discussions and Summary

[23] Comparisons between the present work and those in paper 1 show that the GLOW model is more efficient in providing energy to the thermosphere, especially in the high EUV cases. As discussed in the previous section, the dominant neutral gas heating mechanisms are the exothermic chemical reactions in the lower thermosphere and the electron collisional heating in the upper thermosphere. Both

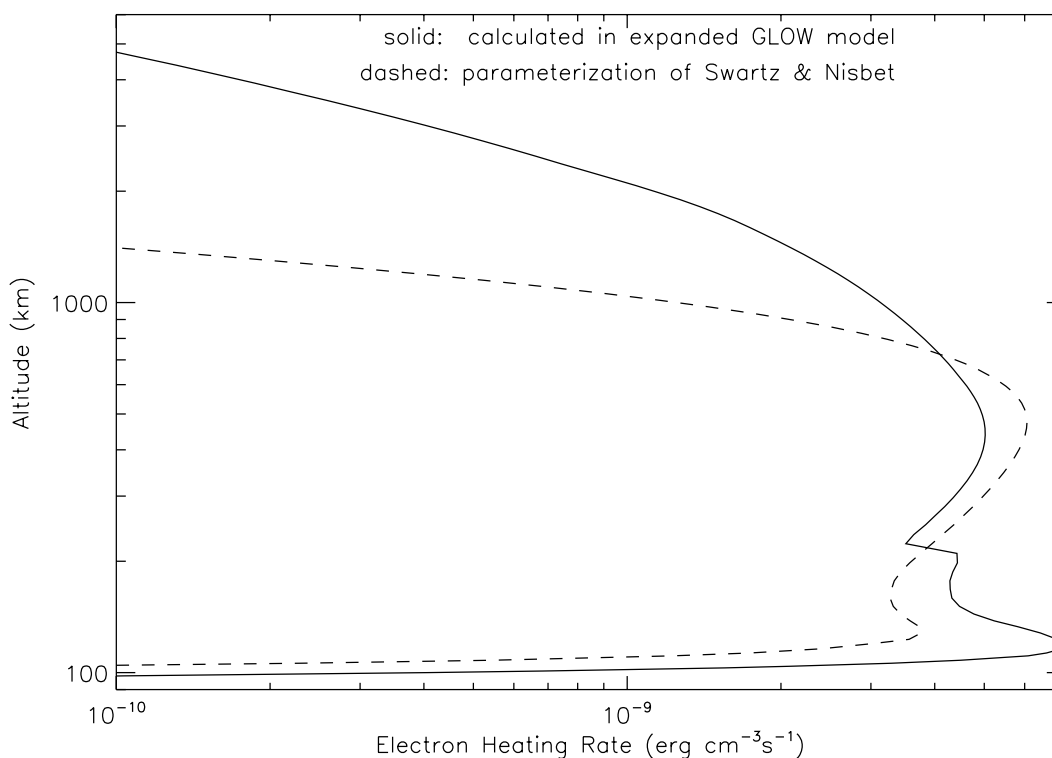


Figure 9. Ambient electron heating rate profiles in the $4.6\times$ present EUV case. The solid curve is calculated in the expanded GLOW model, and the dashed curve is from the *Swartz and Nisbet* [1972] parameterization.

mechanisms depend on temperature (of neutral, ion, and electrons) and composition.

[24] The energy source of the ambient electrons, which is the major heating source of the neutral and ion gases in the upper thermosphere, is from the photoelectrons. The parameterization by *Swartz and Nisbet* [1972] is used to compute the ambient electron heating rate in model 1, as well as in general circulation models such as the thermosphere-ionosphere-mesosphere-electrodynamics general circulation model (TIME-GCM) [*Roble and Ridley*, 1994; *Roble*, 1995] and the TIE-GCM model [*Richmond et al.*, 1992; *Wang et al.*, 2006]. The GLOW model calculates the collisions between photoelectrons and the ambient electrons explicitly. In Figure 9 the ambient electron heating rate calculated in the GLOW model (solid curve) is compared with that from that obtained from the *Swartz and Nisbet* parameterization (dashed curve) in the $4.6\times$ present EUV case. It is clear that in the region where the electron collisional heating dominates the neutral gas heating ($>\sim 1000$ km altitude), the GLOW model provides much more ambient electron heating than the parameterization of *Swartz and Nisbet* [1972] does. This is in agreement with the finding of *Smithro and Sojka* [2005] that the ambient electron heating rate in the GAIT model is 40% greater than that provided by *Swartz and Nisbet's* [1972] parameterization. To test the model's sensitivity to the ambient electron heating treatments, we use the *Swartz and Nisbet* parameterization instead of the GLOW calculated ambient electron heating rates while keep using the ionization, excitation, and dissociation rates provided by GLOW. The exobase temperatures as a function of solar EUV energy fluxes are plotted

as the dotted curve in Figure 10. In comparison, the dashed curve is from paper 1, and the solid curve is obtained by using the GLOW calculated ambient electron heating rates. The dotted curve remains close to the dashed curve until the solar EUV flux reaches $\sim 4\times$ present level. This suggests that the GLOW-calculated ambient electron heating rates is not the main source of extra energy in these cases. The dotted curve deviates from the dashed curve significantly for $>4\times$ present EUV cases, suggesting that the enhanced, GLOW-calculated ambient electron heating is important in correctly understanding the thermosphere energy budget in extreme solar EUV conditions. Figure 10 also better demonstrates that the exobase temperature in the present work starts to decrease with increasing EUV flux at $\sim 4\times$ present EUV condition, which is strong evidence that the thermosphere moves from a hydrostatic regime into a hydrodynamic regime.

[25] The discontinuity at ~ 200 km altitude in the model calculated ambient electron heating rate (solid curve in Figure 9) is caused by using a coarse energy grid ($\Delta E = 0.5$ eV) in the GLOW model, which makes photoelectrons with energy less than 0.25 eV unable to heat ambient electrons where electron temperature rises above ~ 3000 K. The average energy of ambient electrons is ~ 0.26 eV. The ambient electrons may give energy to the photoelectrons with energy lower than 0.25 eV, a cooling effect for the ambient electrons. However, the photoelectron population is so small compared with the ambient electrons that this cooling effect should be negligible. Simulations with much finer electron energy grid ($\Delta E = 0.1$ eV) show better overall shape for the ambient electron heating rates and

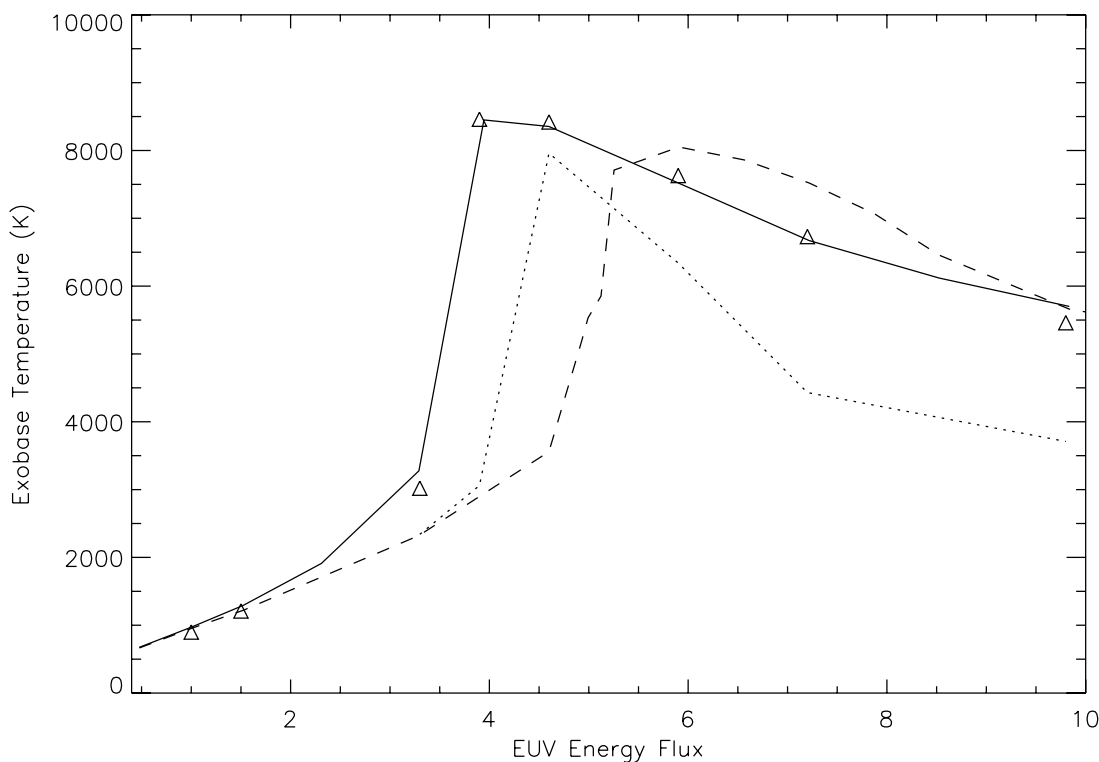


Figure 10. Exobase temperatures under different solar EUV conditions. The solid curve represents those computed in this work. The dashed curve is from model 1. The dotted curve is computed in this work but using the Swartz and Nisbet parameterization instead of the GLOW model calculations for the ambient electron heating. The triangles are the simulations results in this work without the contributions from the Joule heating.

produce similar results as those from using the coarse grid system. Our model shows that with the finer energy grid, the ambient electron heating rate in the solar maximum case decreases significantly in the lower thermosphere (up $\sim 25\%$ at ~ 130 km) but decreases only slightly in the upper thermosphere ($< 5\%$ above 200 km). Because the electron collisional heating becomes the dominant neutral heating term only in altitude greater than ~ 300 km altitude in the solar maximum case (Figure 5), the reduction of the ambient electron heating rate by using a finer electron energy grid only leads to a decrease of the exobase neutral temperature by $< 1\%$ in the solar maximum case. Our model shows a $\sim 3\%$ change of the exobase neutral temperature in the $10\times$ present EUV case when increasing the electron energy grid resolution in the range of 0 to 2 eV. Thus the effect of the electron energy grid resolution is negligible when discussing the thermospheric neutral temperature structure.

[26] Because the solid curve in Figure 10 deviates from the dotted and the dashed curves for solar EUV fluxes $< 4\times$ present level, the GLOW provided ionization and dissociation rates must be the main contributor of the enhanced neutral heating. The expanded GLOW model computes the ionization of atomic nitrogen by electron impact processes. This effect cannot be treated using the parameterization method derived from the original GLOW model. However, because atomic nitrogen remains a minor gas throughout the thermosphere in $< 4\times$ present EUV flux cases (Figure 7), the enhanced neutral heating is unlikely to be due to the

ionization of atomic nitrogen and thus must be from the usage of the GLOW model. Figure 10 suggests that this enhancement of the neutral heating begins to be important at $\sim 3\times$ present EUV condition. Thus the parameterization by *Solomon and Qian* [2005] may not be applicable to conditions where the solar EUV fluxes exceed $\sim 3\times$ present level.

[27] Although the ionization of atomic nitrogen does not contribute to the enhancement of neutral gas heating in the moderate solar EUV cases, it can be important for extreme solar EUV conditions. Figure 7 shows that N^+ is the dominant ion species between ~ 300 km and 2000 km in the $10\times$ present EUV case. Figure 8 shows that the photoelectron enhancement factors of atomic nitrogen is greater than 1 in the lower thermosphere (< 500 km) in the $10\times$ present EUV case, indicating an important contribution to the formation of N^+ from the electron impact process. Thus under the extreme EUV conditions, the inclusion of electron impact ionization of atomic nitrogen can increase its ionization rates and the electron density in the thermosphere, leading to more chemical and electron collisional heating of the neutral gases.

[28] To test the model's sensitivity to the adiabatic cooling in the energy equation of electron gas, we run the model without the adiabatic cooling term in the $4\times$ and $10\times$ present EUV cases. The model calculated exobase temperatures change from 5700 K to 5800 K (2% increase) in the $10\times$ case and no significant difference in the $4\times$ case. Thus adiabatic cooling does not play an important role in electron

gas energy budget if electrons move at the same bulk motion velocity as neutral and ion species.

[29] The top boundary condition for the electron gas energy equation is a fixed downward heat flux of $3 \times 10^9 \text{ eV cm}^{-2} \text{ s}^{-1}$. A heat flux of comparable magnitude is required in the current model (hydrodynamic thermosphere/ionosphere model in combination with the expanded GLOW model) to duplicate the upper thermosphere electron temperature structure in present Earth's thermosphere, similar to the findings of previous results [Roble *et al.*, 1987; Roble, 1995; Smithtro and Sojka, 2005]. The possible sources of this energy are still under debate [Wang *et al.*, 2006]. If we assume that this heat flux should be proportional to the incoming solar EUV energy flux, as that done by Smithtro and Sojka [2005], a heat flux of $3 \times 10^{10} \text{ eV cm}^{-2} \text{ s}^{-1}$ should be applied to the $10\times$ present EUV case. Simulations show that this heat flux enhancement leads to $\sim 15\%$ increase of the neutral gas temperature in upper thermosphere. It is important to realize that under extreme solar EUV conditions, the exobase expands to large distances (4 Earth radii in the $10\times$ present EUV case), in which case, magnetospheric features such as the radiation belt and ring current may disappear completely or change their characteristics dramatically. Researches of the magnetosphere are needed in order to better constrain this boundary condition.

[30] We note that under extreme solar EUV conditions the exobase of the Earth's atmosphere would have expanded to several Earth's radii and the plasma density could have been comparable to the neutral density. Considering the strong solar wind from a young Sun, the magnetosphere of the Earth could have been significantly more compressed billions of years ago. It is likely that the magnetospheres of early terrestrial planets shared the same space with a much extended thermosphere and ionosphere. Yamauchi and Wahlund [2007] analyzed the nonlinear response of the ionosphere to solar parameters and discussed its influences to the atmospheric escape processes. Although to estimate atmospheric escape rates is not the focus of this manuscript, we note that the interactions of the early solar wind with the neutral atmosphere and ionosphere of early terrestrial planets, as well as the efficiencies of various types of atmospheric escape processes, would have been significantly influenced by the dramatic expansion of the thermosphere/ionosphere, in agreement with Lammer *et al.* [2006], Kulikov *et al.* [2006, 2007], and Güdel [2007].

[31] We note that a certain dip angle is employed in the GLOW model and electrons are assumed to be moving along with ions in the hydrodynamic model, which are highly simplified assumptions and present certain degree of inconsistency. To build a fully self-consistent picture and to learn the details of the thermosphere-ionosphere-magnetosphere system require future 3-D simulations. Nevertheless, physical processes in the magnetosphere should have been severely influenced by collisional interactions between neutral gases and the plasma, similar to what is going on in the ionosphere of present Earth.

[32] It is important to realize that the atmospheric composition of early Earth was probably different from that of today. Thus the thermospheric structure presented here is for theoretical interests only. However, with the successful coupling between a 1-D, multicomponent, hydrodynamic

thermosphere/ionosphere model and an energetic electron transport model, systematic investigations of the upper planetary atmospheres during their early evolutionary stages can be pursued on a solid ground.

[33] In summary an energetic electron transport/energy deposition model (GLOW) is expanded to include atomic nitrogen and coupled with a 1-D hydrodynamic thermosphere model. The coupled model is used to investigate the response of the Earth's thermosphere under extreme solar EUV conditions and compare with previous studies [Tian *et al.*, 2008]. It is found that (1) the parameterization of Swartz and Nisbet [1972], which is used widely by theoretical models for present Earth's thermosphere, underestimates the ambient electron heating by photoelectrons significantly in the upper thermosphere of the Earth under $>3\times$ present solar EUV conditions; (2) the transition of the Earth's thermosphere from a hydrostatic equilibrium regime to a hydrodynamic regime occurs at a smaller solar EUV flux condition due to enhanced, more realistic and self-consistent, ambient electron heating by photoelectrons and the subsequent neutral heating from ambient electrons; (3) atomic nitrogen becomes the dominant neutral species in upper thermosphere (competing against atomic oxygen), due to enhanced dissociation and much larger scale height of N_2 , under extreme solar EUV conditions, in which situation the electron impact processes of atomic nitrogen become important for both the chemistry and energetics in the corresponding thermosphere/ionosphere; (4) N^+ remains a minor ion comparing with O^+ when atomic nitrogen dominates the exobase, probably caused by ion chemistry; and (5) the adiabatic cooling effect plays a negligible role in the energy budget of the electron gas. All of these findings highlight the importance of including an energetic electron transport/energy deposition model in theoretical investigations of the thermosphere and ionosphere of terrestrial planets in their early evolutionary stages.

[34] **Acknowledgments.** We thank Christopher Smithtro and the other anonymous reviewer for their helpful comments and suggestions, which helped to improve this manuscript. We thank W. B. Wang for helpful discussions. F. Tian thanks the High Altitude Observatory of NCAR for providing the computing facilities. F. Tian is supported by the NASA Postdoctoral Program through the NASA Astrobiology Institute under Cooperative Agreement CAN-00-OSS-01. S.C.S acknowledges support from NASA grant NNX07AC55G to the National Center for Atmospheric Research. The National Center for Atmospheric Research is supported by the National Science Foundation.

References

- Alexander, M. J., A. I. F. Stewart, S. C. Solomon, and S. W. Bougher (1993), Local-time asymmetries in the Venus thermosphere, *J. Geophys. Res.*, *98*, 10,849, doi:10.1029/93JE00538.
- Avakyan, S. V., et al. (1998), *Collision Processes and Excitation of UV Emission from Planetary Atmospheric Gases*, Gordon and Breach, Amsterdam.
- Bailey, S. M., C. A. Barth, and S. C. Solomon (2002), A model of nitric oxide in the lower thermosphere, *J. Geophys. Res.*, *107*(A8), 1205, doi:10.1029/2001JA000258.
- Fennelly, J. A., and D. G. Torr (1992), Photoionization and photoabsorption cross sections of O, N_2 , O_2 , and N for aeronomic calculations, *At. Data Nucl. Data Tables*, *51*, 321, doi:10.1016/0092-640X(92)90004-2.
- Green, A. E. S., and T. Sawada (1972), Ionization cross sections and secondary electron distributions, *J. Atmos. Terr. Phys.*, *34*, 1719, doi:10.1016/0021-9169(72)90031-1.
- Green, A. E. S., and R. S. Stolarski (1972), Analytic models of electron impact excitation cross sections, *J. Atmos. Terr. Phys.*, *34*, 1703, doi:10.1016/0021-9169(72)90030-X.

- Güdel, M. (2007), The Sun in time: Activity and environment, *Living Rev. Sol. Phys.*, 4, Paper 3.
- Hedin, A. E. (1991), Extension of the MSIS thermosphere model into the middle and lower atmosphere, *J. Geophys. Res.*, 96, 1159, doi:10.1029/90JA02125.
- Jackman, C. H., R. H. Garvey, and A. E. S. Green (1977), Electron impact on atmospheric gases: 1. Updated cross sections, *J. Geophys. Res.*, 82, 5081.
- Kulikov, Y. N., et al. (2006), Atmospheric and water loss from early Venus, *Planet. Space Sci.*, 54, 1425, doi:10.1016/j.pss.2006.04.021.
- Kulikov, Y. N., H. Lammer, H. I. M. Lichtenegger, T. Penz, D. Breuer, T. Spohn, R. Lundin, and H. K. Biernat (2007), A comparative study of the influence of the active young Sun on the early atmospheres of Earth, Venus, and Mars, *Space Sci. Rev.*, 129, 207, doi:10.1007/s11214-007-9192-4.
- Lammer, H., Y. N. Kulikov, and H. I. M. Lichtenegger (2006), Thermospheric X-ray and EUV heating by the young Sun on early Venus and Mars, *Space Sci. Rev.*, 122, 189, doi:10.1007/s11214-006-7018-4.
- Meier, R. R. (1991), Ultraviolet spectroscopy and remote sensing of the upper atmosphere, *Space Sci. Rev.*, 58, 1, doi:10.1007/BF01206000.
- Nagy, A. F., and P. M. Banks (1970), Photoelectron fluxes in the ionosphere, *J. Geophys. Res.*, 75, 6260, doi:10.1029/JA075i031p06260.
- Richmond, A. D., E. C. Ridley, and R. G. Roble (1992), A thermosphere/ionosphere general circulation model with coupled electrodynamics, *Geophys. Res. Lett.*, 19, 601, doi:10.1029/92GL00401.
- Roble, R. G. (1995), Energetics of the mesosphere and thermosphere, in *The Upper Mesosphere and Lower Thermosphere: A Review of Experiment and Theory*, *Geophys. Monogr. Ser.*, vol. 87, edited by R. M. Johnson and T. L. Killeen, p. 1, AGU, Washington, D. C.
- Roble, R. G., and E. C. Ridley (1994), Thermosphere-ionosphere-mesosphere-electrodynamics general circulation model (TIME-GCM): Equinox solar min simulations, 30–500 km, *Geophys. Res. Lett.*, 21, 417, doi:10.1029/93GL03391.
- Roble, R. G., E. C. Ridley, and R. E. Dickinson (1987), On the global mean structure of the thermosphere, *J. Geophys. Res.*, 92, 8745, doi:10.1029/JA092iA08p08745.
- Sawada, T., D. J. Strickland, and A. E. Green (1972), Electron energy deposition in CO₂, *J. Geophys. Res.*, 77, 4812, doi:10.1029/JA077i025p04812.
- Schunk, R. W., and A. F. Nagy (2000), *Ionospheres: Physics, Plasma Physics, and Chemistry*, Cambridge Univ. Press, New York.
- Smithtro, C. G., and J. J. Sojka (2005), A new global average model of the coupled thermosphere and ionosphere, *J. Geophys. Res.*, 110, A08305, doi:10.1029/2004JA010781.
- Solomon, S. C. (1993), Auroral electron transport using the Monte Carlo method, *Geophys. Res. Lett.*, 20, 185, doi:10.1029/93GL00081.
- Solomon, S. C. (2001), Auroral particle transport using Monte Carlo and hybrid methods, *J. Geophys. Res.*, 106, 107, doi:10.1029/2000JA002011.
- Solomon, S. C., and V. J. Abreu (1989), The 630 nm dayglow, *J. Geophys. Res.*, 94, 6817, doi:10.1029/JA094iA06p06817.
- Solomon, S. C., and L. Qian (2005), Solar extreme-ultraviolet irradiance for general circulation models, *J. Geophys. Res.*, 110, A10306, doi:10.1029/2005JA011160.
- Solomon, S. C., P. B. Hays, and V. J. Abreu (1988), The auroral 6300Å emission: Observations and modeling, *J. Geophys. Res.*, 93, 9867, doi:10.1029/JA093iA09p09867.
- Solomon, S. C., S. M. Bailey, and T. N. Woods (2001), Effect of solar soft X-rays on the lower ionosphere, *Geophys. Res. Lett.*, 28, 2149, doi:10.1029/2001GL012866.
- Stone, E. J., and E. C. Zipf (1973), Excitation of atomic nitrogen by electron impact, *J. Chem. Phys.*, 58, 4278, doi:10.1063/1.1678984.
- Swartz, W. E., and J. S. Nisbet (1972), Revised calculations of F region ambient electron heating by photoelectrons, *J. Geophys. Res.*, 77, 6259.
- Tayal, S. S., and O. Zatsarinny (2005), B-spline R-matrix with pseudostates approach for electron impact excitation of atomic nitrogen, *J. Phys. B At. Mol. Opt. Phys.*, 38, 3631, doi:10.1088/0953-4075/38/20/001.
- Tian, F., J. F. Kasting, H.-L. Liu, and R. G. Roble (2008), Hydrodynamic planetary thermosphere model: 1. Response of the Earth's thermosphere to extreme solar EUV conditions and the significance of adiabatic cooling, *J. Geophys. Res.*, 113, E05008, doi:10.1029/2007JE002946.
- Wang, W., A. G. Burns, and T. L. Killeen (2006), A numerical study of the response of the ionospheric electron temperature to geomagnetic activity, *J. Geophys. Res.*, 111, A11301, doi:10.1029/2006JA011698.
- Yamauchi, M., and J.-E. Wahlund (2007), Role of the ionosphere for the atmospheric evolution of planets, *Astrobiology*, 7, 783, doi:10.1089/ast.2007.0140.
- Zipf, E. C., and P. W. Erdman (1985), Electron impact excitation of atomic oxygen: Revised cross sections, *J. Geophys. Res.*, 90, 11087, doi:10.1029/JA090iA11p11087.

J. Lei, L. Qian, R. G. Roble, S. C. Solomon, and F. Tian, High Altitude Observatory, National Center for Atmospheric Research, Boulder, CO 80307, USA. (tian@ucar.edu)